Supplementary Data

Development of adsorbents based on phosphate-containing hyper-cross-linked polymers for selective removal of tetracycline from water: unveiling the role of phosphate groups in adsorption

Joanna Wolska[a,b,*], Anetta Zioła-Frankowska[a], Jacek Jenczyk[c], Adrian Zaleta[a], Kamila Sobańska[b], Piotr Pietrzyk[b], Lukasz Wolski[a]

[a] *Faculty of Chemistry, Adam Mickiewicz University, Poznań, ul. Uniwersytetu Poznańskiego 8, 61-614 Poznań, Poland*

[b] *Faculty of Chemistry, Jagiellonian University, ul. Gronostajowa 2, 30-387 Kraków, Poland*

[c] *NanoBioMedical Centre, Adam Mickiewicz University, Poznań, ul. Wszechnicy Piastowskiej 3, 61-614 Poznań, Poland*

Table of content

1. Extended experimental section

1.1. Synthesis of hyper-cross-linked polymers

The yield of hyper-cross-linked polymer synthesis was calculated using the following equation (Eq. S1):

$$Yield = \frac{m_{polymer}}{m_{monomers}} \times 100\% \qquad \text{(Eq. S1)}$$

Where $m_{polymer}$ and $m_{monomers}$ stand for the weight of the dry polymer and the weight of the BCMB and DPP monomers, respectively. Additionally, $m_{polymer}$ includes the $m_{monomer}$ and the mass of the ethylene cross-linking bridges formed as a by-product of Friedel-Crafts alkylation with the solvent (DCE) [*Macromolecules* 57 (2024) 5507, doi: 10.1021/acs.macromol.4c00503] with a small residue of chlorine, as confirmed by XPS analysis (see Table S3). The chlorine species may originate from terminated chloroalkyl groups (–CH_2Cl and/or –CH_2CH_2Cl), derived from both BCMB and DCE. Consequently, the yield of HCPs may exceed 100% [*Adv. Mater.* (2024) 2307579, doi: 10.1002/adma.202307579; *ACS Appl. Mater. Inter.* 14 (2022) 7369, doi: 10.1021/acsami.1c24393].

1.2. Estimating the cost of adsorbent preparation

Estimated costs per gram of P1-HCP material have been calculated using the reagents required for its synthesis (see Experimental Methods, pages 5-6). Unit prices found on Merck's website (www.sigmaaldrich.com/PL/pl) as of March 9, 2025 were used for all calculations. A minimum reagent purity of ≥95% was required. Work-up steps, such as washing, were excluded from the calculations as quantities of work-up reagents are often not disclosed, hence, estimating cost is not possible. The operating time, synthesis time, and power were also not factored into the calculation. A detailed breakdown of the estimated costs is provided in Table S1 shown below. The total cost of this P1-HCP material only takes into account lab-scale production.

Table S1. Detailed breakdown of the estimated cost of preparing 1 gram of P1-HCP1.

Reagent	Unit Price (€) (Quantity/Volume)	Reagent Quantity/Volume for 1 g of Polymer	Price of Reagent per 1 g of Polymer (€)
4,4'-bis(chloromethyl)-1,1'-biphenyl	98 (250 g)	0.9 g	0.3
diphenyl phosphate	207 (25 g)	0.4 g	3.5
1,2-dichloroethane	249 (1000 mL)	41.0 mL	10.1
ferric chloride	92 (1000 g)	3.3 g	0.3
Total cost of preparing of P1-HCP adsorbent (€/g)			**14.3**

1.3. Characterization of HCP-based adsorbents

Solid-state ^{13}C NMR spectra were acquired at ambient conditions on a 400 MHz Agilent spectrometer equipped with Wide Bore Triple Resonance T3 MAS XY probe. Samples were placed into a 4 mm diameter zirconia rotor. Spectra were recorded using Cross-Polarization (CP) sequence with CP contact time set to 1550 μs. ^{13}C detection with dipolar decoupling of protons was used. Experiments were performed under magic angle spinning (MAS) conditions with a spinning frequency of 10 kHz. 4000 transients were accumulated for each spectrum.

Attenuated total reflectance Fourier transform infrared (ATR-FTIR) spectra of the polymers were acquired in the range of 4000 cm^{-1} to 400 cm^{-1} (resolution 4 cm^{-1}, number of scans = 64) using an IRSpirit-X spectrophotometer (Shimadzu) equipped with attenuated total reflectance (QATR-S) module (Shimadzu).

X-ray photoelectron spectroscopy (XPS) was performed using an ultra-high vacuum photoelectron spectrometer based on a Phoibos150 NAP analyzer (Specs, Germany). The analysis chamber was operated under vacuum with a pressure close to 5×10^{-9} mbar and the sample was irradiated with a monochromatic AlKα (1486.6 eV) radiation. Any charging that might occur during the measurements (due to incomplete neutralization of ejected surface electrons) was accounted for by rigidly shifting the entire spectrum by a distance needed to set the binding energy of the C 1s assigned to adventitious carbon to the assumed value of 284.8 eV.

Elemental analysis (EA) of the HCPs was carried out with an Elementar Analyser Vario EL III. The samples were weighed in tin capsules (4 mg) and introduced into the reactor with a precisely defined portion of oxygen. After combustion at 900-1000 °C, the exhaust gases were transported in helium flow to the second reactor, and then through the water trap to the chromatographic column, which separated the generated gases. Finally, the separated

gases were detected by a thermal conduction detector (TCD). The measurements were repeated three times for each investigated sample.

The quantitative detection of phosphorus and iron involved digesting the polymer samples using a piranha solution, prepared by mixing concentrated sulfuric acid and hydrogen peroxide in a 3:1 volume ratio (v:v). The resulting solution was then diluted with deionized (DI) water, and the phosphorus and iron content was analyzed using inductively coupled plasma optical emission spectrometry (ICP-OES).

Scanning electron microscopy (SEM) images combined with energy dispersive X-ray spectroscopy (EDS) were recorded using a Quanta 250 FEG, FEI instrument. Samples were mounted on carbon tape on aluminium stubs, without any coating treatment.

N_2 adsorption-desorption isotherms were obtained at –196 °C using an Autosorb iQ Analyzer (Quantachrome). Before measurements, the samples were degassed at 80 °C for 22 h. The specific surface area of the materials obtained was calculated by the Brunauer-Emmett-Teller (BET) method, and the average pore size was estimated by the Barrett-Joyner-Halenda (BJH) method from the desorption branch of the isotherm.

Thermogravimetric analysis (TGA) experiments of polymers were performed with a STA 6000 apparatus from Perkin Elmer, under a nitrogen atmosphere, at the heating rate of 10 °C/min from room temperature up to a maximum of 900 °C.

The zeta potential measurements as a function of the pH of aqueous dispersions of the HCP and P1-HCP polymers ($C_{polymer}$ = 1 g/L) were carried out using a Zetasizer Nano ZS (Malvern). The zeta potential was estimated from electrophoretic mobility using the Henry equation: $U_E = 2\varepsilon\zeta F(\mathrm{ka})/3\eta$, where U_E represents the electrophoretic mobility, ζ is the zeta potential, ε denotes the dielectric constant, $F(\mathrm{ka})$ is Henry's function (set to 1.5 as in the Smoluchowski approximation), and η is the viscosity. The pH was adjusted using 0.5 mol/L solutions of HCl or NH_3 in H_2O.

1.4. Adsorption experiments

The efficiency of tetracycline removal from tap water carried out using very low (trace) concentration of the antibiotic (50 or 100 μg/L) was performed using LC–MS/MS included a Shimadzu Liquid Chromatography system coupled to a Shimadzu 8050 triple quadrupole mass spectrometer (Shimadzu, Japan). Optimized MRM transitions for tetracycline were as follows: 445.4-410.0, 445.4-154.0. The UHPLC system consisted of a solvent delivery system (two pumps Nexera X2 LC-30AD), an autosampler (Nexera X2 SIL-30AC), degasser (DGU-20A5R), a column oven (CTO-20AC) and a system controller (CBM-20A). Compounds were chromatographically separated on a Kinetex C18 (2.1 × 100 mm, 2.6 μm) column with isocratic elution using (A) water (0.1% formic acid) and (B) acetonitrile (0.1% formic acid) as mobile phases A and B (60%:40%), respectively. The flow rate was 0.4 mL/min, and the total run time was 5.0 min. Operating conditions of the mass spectrometer were as follows: Ionization: ESI positive; DL temp.: 250 °C; Interface temp.: 300 °C; Block heater temp.: 500 °C; Nebulizer gas flow: 3 L/min; Drying gas flow: 10 L/min; Heating gas flow: 10 L/min; Dwell time: 20 ms; Pause time: 1 ms. Standards solutions were prepared from tetracycline with the concentration of 1000 mg/L in methanol (Merck, Poland) for LC-MS/MS.

Adsorption kinetic parameters were determined by using linearized form of the pseudo-first order (PFO) (Eq. S2) and pseudo-second order (PSO) (Eq. S3) models described by Ho and McKay [*Process Biochem.* 34 (1999) 451, doi: 10.1016/S0032-9592(98)00112-5], where $q(t)$ and q_e are the amount of adsorbate adsorbed at any given time, t and at equilibrium, respectively, k_1 and k_2 corresponds to adsorption rate constant for pseudo-first order and pseudo-second order model, respectively.

$$\ln\left(q_e - q(t)\right) = -k_1 t + lnq_e \qquad \text{(Eq. S2)}$$

$$\frac{t}{t(q)} = \left(\frac{1}{q_e}\right) t + \frac{1}{k_2 q_e^2} \qquad \text{(Eq. S3)}$$

k_1 and k_2 values were determined by plotting $\ln(q_e - q(t))$ vs t and $\frac{t}{t(q)}$ vs t for PFO and PSO, respectively. The kinetics parameters were then estimated from the slope and intercept of the best fit line such that, if m = slope and b = intercept, $k_1 = -m$ and $q_e = exp\ (b)$ for PFO, while $k_2 = \frac{m^2}{b}$ and $q_e = m^{-1}$ for PSO [*Clean. Eng. Technol.* 1 (2020) 100032, doi: 10.1016/j.clet.2020.100032]. Additionally, experimental data were also fitted to the non-linear forms of PFO and PSO models [*Surf. Interfaces* 22 (2021) 100806, doi: 10.1016/j.surfin.2020.100806].

Experimental q_e values were estimated on the basis of adsorption tests using the following formula (Eq. S4):

$$q_e = \frac{V(C_0 - C_t)}{m} \qquad \text{(Eq. S4)}$$

where, C_0 is an initial concentration of drug (mg/L), C_t is concentration of drug (mg/L) after a given adsorption time, t (min), V is the volume of the reaction mixture (L), and m is the mass of the adsorbent (g).

Adsorption kinetics was also analyzed using Weber–Morris intraparticle diffusion (IPD) model (Eq. S5) [*J. Sanit. Eng. Div. Am. Soc. Civ. Eng.* 89 (1963) 31, doi: 10.1061/JSEDAI.0000430].

$$q_t = K_{id} t^{\frac{1}{2}} + C \qquad \text{(Eq. S5)}$$

where q_t is the adsorption capacity at any time (mg/g), K_{id} is the intraparticle diffusion rate constant (mg g^{-1} $min^{-1/2}$), t is the time taken for the adsorption process (min) and C is a constant for the any experiment (mg/g) that gives an idea about the thickness of the boundary layer. When a graph of q_t is plotted against $t^{\frac{1}{2}}$, a linear graph is obtained with regression linear coefficient, R^2, close to unity. The slope of the graph reveals the intraparticle diffusion rate constant, K_{id}, while intercept of the graph stands for C.

Isotherms of the tetracycline adsorption were recorded in the bath mode using an Easy Max 102 Advanced Thermostat system (Mettler Toledo). Experimental data were fitted to Langmuir and Freundlich adsorption models. Adsorption isotherm parameters were determined by using linearized form of the Langmuir (Eq. S6) and Freundlich (Eq. S7) [*SN Appl. Sci.* 2 (2020) 187, doi: 10.1007/s42452-020-1978-y].

$$\frac{C_e}{q_e} = \frac{1}{q_m}(C_e) + \frac{1}{q_m K_L} \qquad \text{(Eq. S6)}$$

$$\log_{10} q_e = \frac{1}{n}\log_{10} C_e + \log_{10} K_F \qquad \text{(Eq. S7)}$$

In the case of linear form of Langmuir model (Eq. S6), q_e is the amount of adsorbate per unit mass of adsorbent at equilibrium (mg/g), K_L is the adsorption capacity constant (L/g), C_e is the concentration of adsorbate at equilibrium (mg/L) and q_m is the maximum adsorption capacity (mg/g). When graph of $\frac{C_e}{q_e}$ is plotted against C_e, a linear graph is a acquired with regression linear coefficient, R^2, close to unity. The q_m and K_L are obtained from the slope and intercept of the graph. Both the slope and intercept of the graph represent the values for $\frac{1}{q_m}$ and $\frac{1}{q_m K_L}$, respectively.

In the case of linear form of Freundlich model (Eq. S7), where q_e is the amount of adsorbate per unit mass of adsorbent at equilibrium (mg/g), K_F is the adsorption capacity constant (L/g), C_e is the concentration of the adsorbate at equilibrium (mg/L), n is the heterogeneity factor and $\frac{1}{n}$ is the adsorption intensity. When a graph of $\log_{10} q_e$is plotted against $\log_{10} C_e$, a linear graph is acquired with regression linear coefficient, R^2, close to unity. The n and K_F are obtained from the slope and intercept of the graph. Both the slope and intercept of the graph represent the values for $\frac{1}{n}$ and $\log_{10} K_F$, respectively.

Additionally, experimental data were also fitted to the non-linear forms of Langmuir and Freundlich isotherm adsorption models [*Surf. Interfaces* 22 (2021) 100806, doi: 10.1016/j.surfin.2020.100806].

Gibbs free energy (ΔG^0), was determined according to Eq. (S8).

$$\Delta G = -RT \ln(K_L) \qquad \text{Eq. (S8)}$$

where, T is the solution temperature (K, 20°C), R is the ideal gas constant (8.314 J mol^{-1} K^{-1}) and K_L is the adsorption capacity constant (L/g) derived from Langmuir isotherm model. Since K_L should be unitless to get the correct units, the Langmuir isotherm coefficient K_L was converted into a dimensionless constant by multiplying it by 1000 [*J. Serb. Chem. Soc.* 72 (2007) 1363, doi: 10.2298/JSC0712363M].

Activation energy (E_a) was calculated using the linear form of Arrhenius equation (Eq. S9):

$$\ln k = -\frac{E_a}{RT} + \ln A \qquad \text{(Eq. S9)}$$

where, E_a (J mol^{-1}) is the apparent activation energy of the reaction; R is the ideal gas constant (8.314 J mol^{-1} K^{-1}), T is reaction temperature (K), k is a coefficient. Since the adsorption process is in accordance with pseudo-second order kinetic model, the apparent activation energy was calculated by the coefficient of k derived from pseudo-second order kinetic model. When a graph of $\ln k$ is plotted against $1/T$, a linear graph is acquired with regression linear coefficient, R^2, close to unity. The E_a is obtained from the slope of the graph. The slope of the graph represents the values for $-E_a/R$.

1.5. Reuse tests and regeneration procedure

In a standard reuse experiment, 20 mg of P1-HCP (adsorbent loading = 0.10 g/L) was added to 200 mL of TC solution (C_0 = 30 mg/L) and stirred vigorously (600 rpm). After 24 h of agitation at room temperature (adsorption step), the P1-HCP material was separated from the solution through PTFE filter paper (Biosens, 0.22 μm) on a glass vacuum filtration apparatus (Whatman). Concentration of the TC in the filtrate was analyzed on the basis of UV-vis measurements, and the efficiency of antibiotic removal after a given adsorption cycle was determined using equation (Eq. 1, see in main text). To regenerate the spent adsorbent, the polymer collected and separated after the adsorption step was dispersed in 100 mL of a regenerator solution composed of EtOH and 2.0 M HCl in a 1:1 (v:v) ratio and stirred for 3 h at room temperature (stirring rate = 300 rpm). The regenerated polymer was then thoroughly rinsed with deionized water until neutral pH was achieved and subsequently used for the next adsorption cycle. The regeneration performance of P1-HCP was evaluated over five consecutive adsorption-desorption cycles.

Table S2. Main physicochemical properties of real water matrices used for the adsorption experiments.

Parameter (unit)	deionized water	tap water	Warta River
pH	6.8	7.4-7.5	8.0-8.4
Total carbon (mg/L)	0.67	54.14	48.13
Total organic carbon (mg/L)	0.40	<LOD[a]	0.64
Total inorganic carbon (mg/L)	0.26	54.14	47.49
Total nitrogen (mg/L)	0.03	0.74	3.48
Ca^{2+} (mg/L)	0.41	120.10	79.80
Mg^{2+} (mg/L)	0.37	13.21	9.37
Na^{+} (mg/L)	0.13	33.90	45.10
K^{+} (mg/L)	0.03	5.95	91.71

[a] below the limit of detection

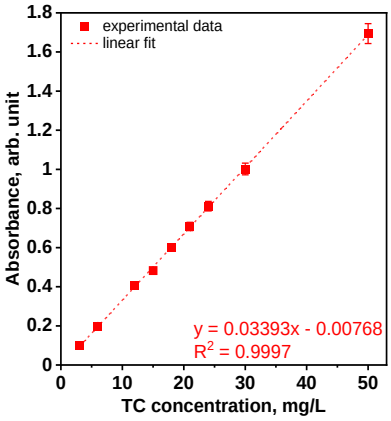

Fig. S1. Relationship between concentration of the TC and its absorbance at λ_{max} = 275 nm.

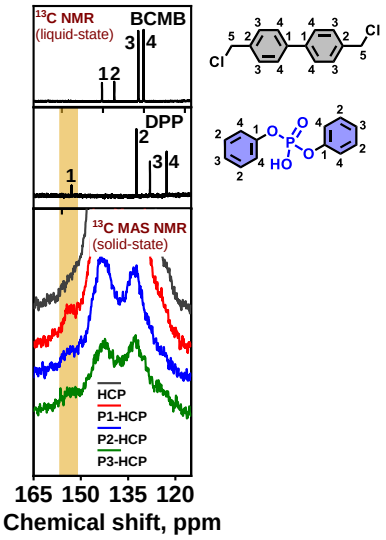

Fig. S2. Comparison of the solid-state ^{13}C MAS NMR spectra of all HCPs with the liquid-state ^{13}C NMR spectra of 4,4'-bis(chloromethyl)-1,1'-biphenyl (BCMB) and diphenyl phosphate (DPP) monomers in $CDCl_3$ solution in the 165–115 ppm region, highlighting the most downfield signal (ca. 150 ppm) observed only in MAS NMR spectra of the P-HCPs, attributed to the aromatic carbons directly bonded to the phosphate groups in DPP unit (orange region). The chemical shifts in the liquid-state ^{13}C NMR spectra of BCMB and DPP monomers are as follows: for BCMB, δ_1 = 143.31, δ_2 = 139.44, δ_3 = 131.78, δ_4 = 130.12, and δ_5 = 48.64 ppm (outside the depicted range; see Fig. 1A); for DPP, δ_1 = 153.00, δ_2 = 132.36, δ_3 = 128.06, and δ_4 = 122.77 ppm.

Table S3. Atomic surface concentration of elements estimated from XPS data using Casa XPS software.

Element	Atomic surface concentration [at.%]			
	HCP	P1-HCP	P2-HCP	P3-HCP
C	94.64	84.39	83.97	79.79
O	2.41	10.28	10.60	11.73
P	-	2.55	2.66	3.68
Cl	2.95	2.78	2.76	4.80
Fe	traces[a]	traces[a]	traces[a]	traces[a]
Fe[b]	0.12	0.23	0.29	0.24

[a] Surface concentration >> 0.50 at.%

[b] Surface concentration of Fe [at.%] determined based on SEM-EDS.

Table S4. Chemical composition of the polymer-based adsorbents.

Polymer	Elemental composition					
	Elemental analysis[a]		ICP-OES[b]		SEM-EDS[c]	
	C [wt.%]	H [wt.%]	P [wt.%]	Fe [wt.%]	Fe [wt.%]	Fe [at.%]
HCP	85.83 ± 0.26	4.99 ± 0.03	-	-	-	-
P1-HCP	71.38 ± 0.09	4.59 ± 0.01	3.15 ± 0.01	1.42 ± 0.01	0.99 ± 0.08	0.23 ± 0.02
P2-HCP	66.95 ± 0.02	4.28 ± 0.06	3.49 ± 0.01	0.78 ± 0.01	1.19 ± 0.09	0.29 ± 0.02
P3-HCP	63.30 ± 0.01	3.95 ± 0.01	5.46 ± 0.01	1.48 ± 0.01	1.01 ± 0.07	0.24 ± 0.02

[a] Average values derived from three measurements based on EA.

[b] Average values derived from three measurements based on ICP-OES.

[c] Content of iron on the surface of polymers determined based on SEM-EDS.

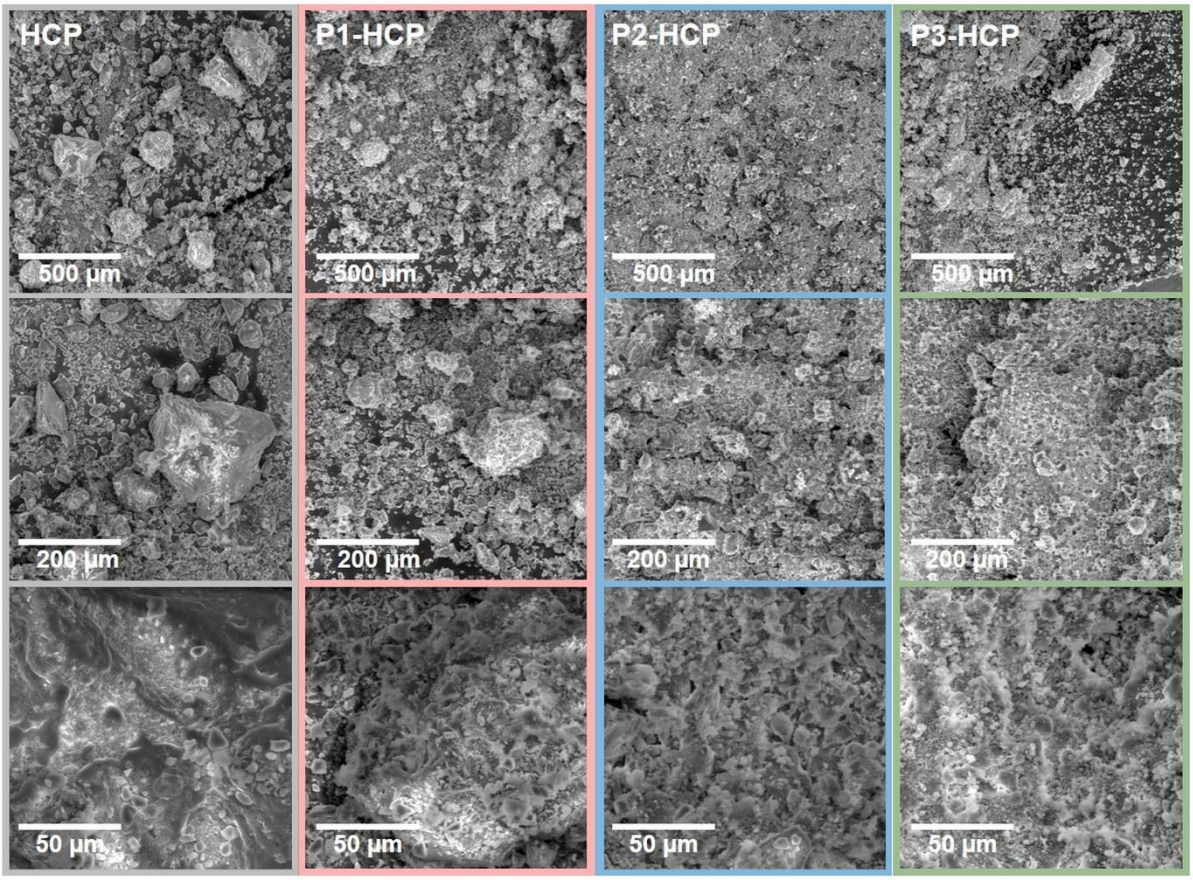

Fig. S3. SEM images of the HCP (grey panel), P1-HCP (red panel), P2-HCP (blue panel), and P3-HCP (green panel) at various magnifications.

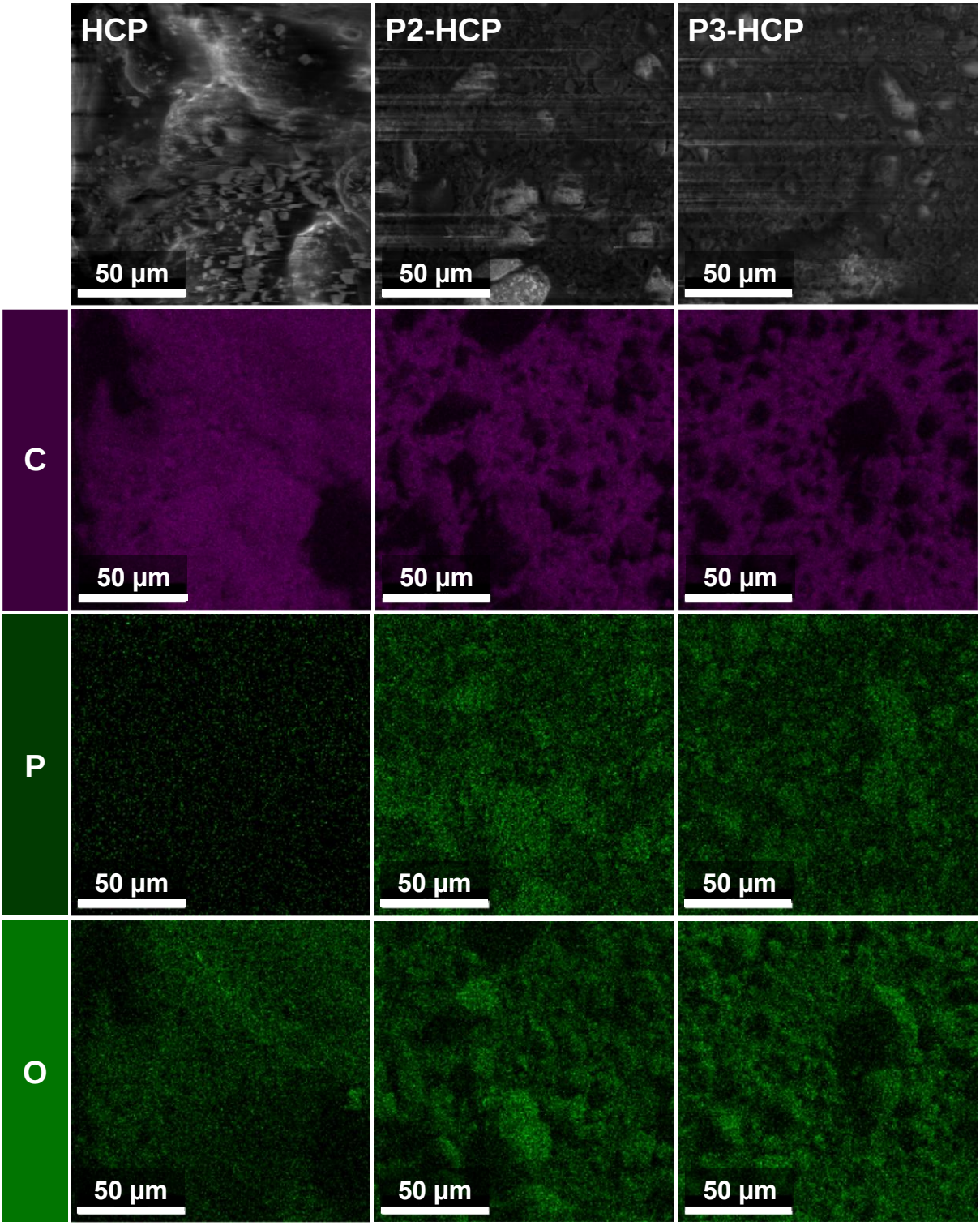

Fig. S4. SEM-EDS elemental mapping for C, P, and O for the HCP (left-hand vertical panel), P2-HCP (middle vertical panel), and P3-HCP (right-hand vertical panel).

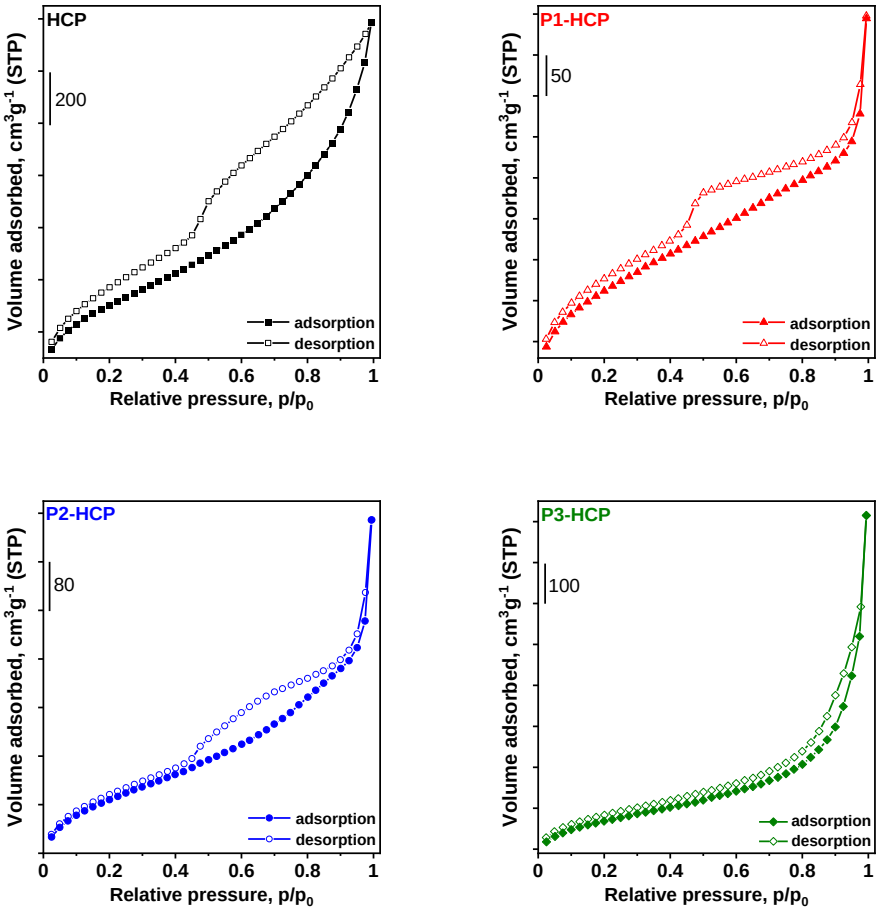

Fig. S5. Low-temperature nitrogen adsorption–desorption isotherms of all investigated HCPs, highlighting the more pronounced changes in the shape of the desorption branch and the hysteresis loop.

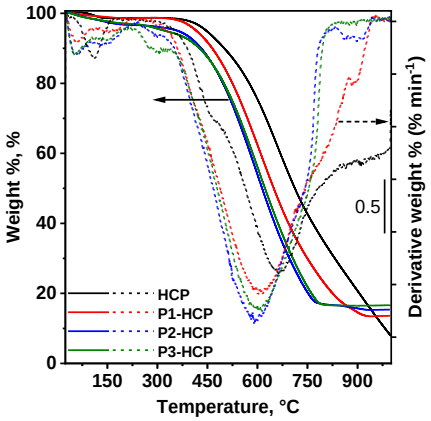

Adsorbent	T_{d10} [°C]
HCP	500
P1-HCP	464
P2-HCP	431
P3-HCP	426

Scheme S1. TGA profile for all HCPs accompanied by a summary of T_{d10} values, which correspond to the temperature at which 10% of the polymer's initial weight is lost.

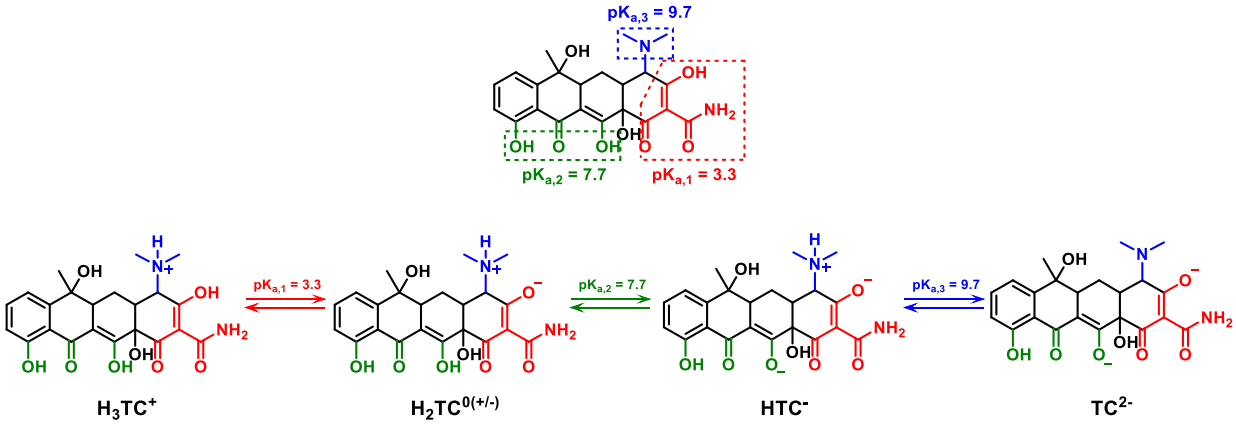

Fig. S6. Speciation of TC at different pH values [*Environ. Sci. Technol.* 48 (2014) 4893, doi: 10.1021/es5003428; *J. Colloid Interf. Sci.* 351 (2010) 254, doi: 10.1016/j.jcis.2010.07.034; *Appl. Clay Sci.* 40 (2008) 179, doi: 10.1016/j.clay.2007.08.003].

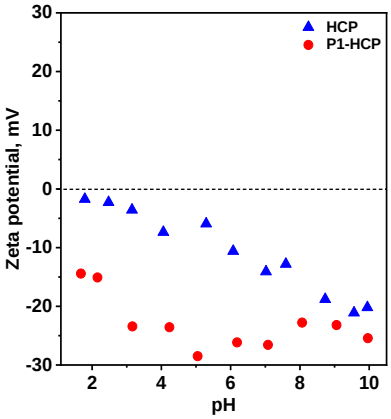

Fig. S7. Surface Zeta potential of P1-HCP and HCP materials at different pH values.

Table S5. TC adsorption kinetic parameters for P1-HCP adsorbent derived from the pseudo-first order (PFO) and pseudo-second order (PSO) linear [*Clean. Eng. Technol.* 1 (2020) 100032, doi: 10.1016/j.clet.2020.100032] and non-linear [*Surf. Interfaces* 22 (2021) 100806; doi: 10.1016/j.surfin.2020.100806] models. Representative graphs used for estimating of the adsorption kinetics are shown in Fig. 8.[a]

Equation type	q_e (exp)[b] [mg/g]	PFO			PSO		
		k [1/min]	q_e(cal)[c] [mg/g]	R^2	k [g/mg/min]	q_e (cal)[c] [mg/g]	R^2
Linear	330.0	0.00379	196.0	0.9795	0.00006	339.0	0.9988
Non-linear		0.02175	283.0	0.8536	0.00010	310.0	0.9417

[a] *Adsorption conditions*: 200 mL of TC solution (C_0 = 20 mg/L), 10 mg of the polymer (adsorbent dosage = 0.05 g/L), initial pH ~ 4.5 (before addition of the adsorbent), room temperature, stirring rate: 600 rpm.

[b] Maximum adsorption capacity of the sample derived from the experiments.

[c] Maximum adsorption capacity of the sample calculated based on a given kinetic model.

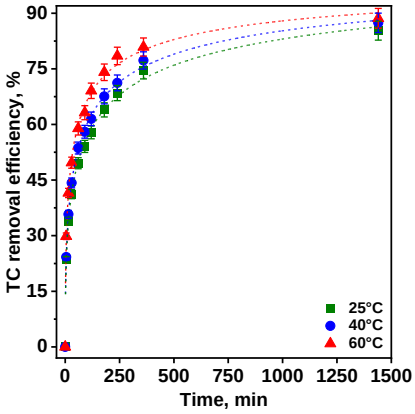

Fig. S8. The effect of temperature on TC removal in the presence of P1-HCP adsorbent. *Adsorption conditions*: 200 mL of TC solution (C_0 = 20 mg/L), 10 mg of the polymer (adsorbent dosage = 0.05 g/L), initial pH ~ 4.5 (before addition of the adsorbent), stirring rate: 600 rpm.

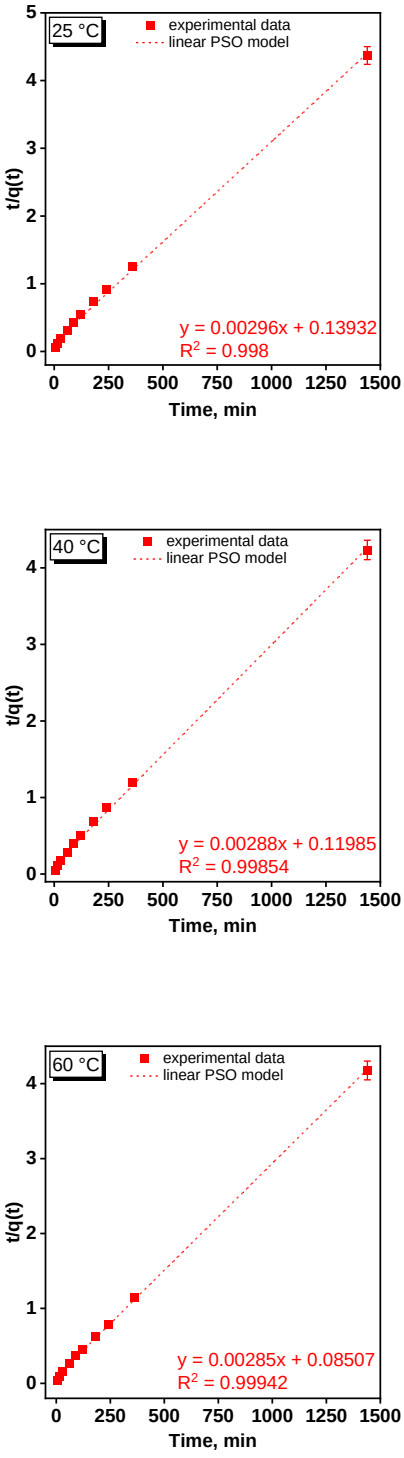

Fig. S9. Graphs used for assessing the pseudo-second order (PSO) kinetic model for the TC adsorption on the P1-HCP adsorbent at different temperature. *Adsorption conditions:* 200 mL of the antibiotic solution (C_0 = 20 mg/L), 10 mg of P1-HCP (adsorbent dosage = 0.05 g/L), initial pH ~ 4.5 (before addition of the adsorbent), stirring rate: 600 rpm.

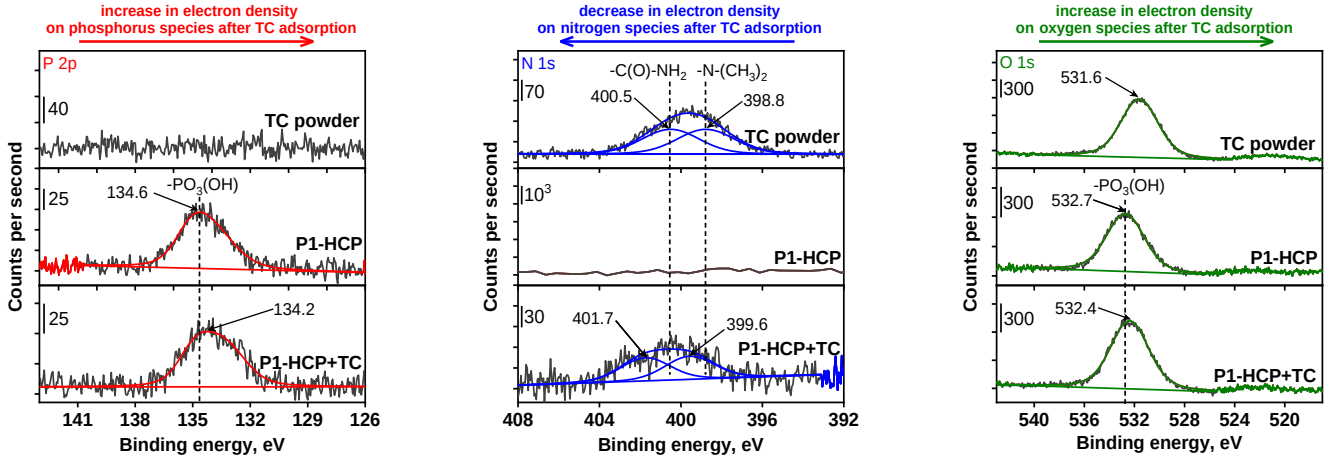

Fig. S10. Comparison of XPS spectra of TC powder, fresh P1-HCP, and P1-HCP after TC adsorption (P1-HCP+TC) in the P 2p, N 1s and O 1s binding energy ranges.

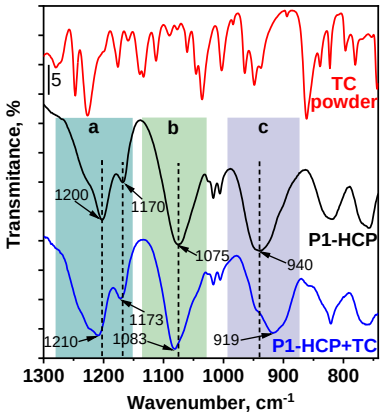

Fig. S11. ATR-FTIR spectra of powdered TC, fresh P1-HCP and spent P1-HCP1 after TC adsorption in the range of 1300-740 cm^{-1}. The highlighted ranges corresponds to the bands attributed to (a) stretching vibrations of the P=O bond (b) stretching vibrations of the P–OH bond, and (c) stretching vibrations of the P–O bond.

Table S6. Main characteristics of five different structure drugs selected to evaluate versatility of P1-HCP adsorbent.

Pharmaceutical Name	Chemical structure	Abbreviation	Chemical formula	Molecular weight [g/mol]	pK_a in RT	References
Antibiotics						
Tetracycline	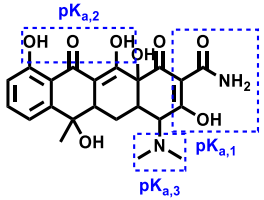	TC	$C_{22}H_{24}N_2O_8$	444.44	3.3 ($pK_{a,1}$) 7.7 ($pK_{a,2}$) 9.7 ($pK_{a,3}$)	*Environ. Sci. Technol.* 48 (2014) 4893, doi: 10.1021/es5003428
Ciprofloxacin	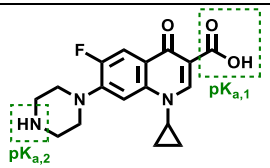	CIP	$C_{17}H_{18}FN_3O_3$	331.35	5.9 ($pK_{a,1}$) 8.9 ($pK_{a,2}$)	*J. Ind. Eng. Chem.* 93 (2021) 57, doi: 10.1016/j.jiec.2020.09.023
Non-steroidal inflammatory drugs						
Diclofenac	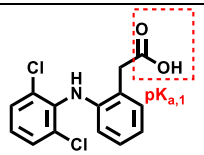	DCF	$C_{14}H_{11}Cl_2NO_2$	296.15	4.0 ($pK_{a,1}$)	*Environ. Earth Sci.* 79 (2020) 277, doi: 10.1007/s12665-020-09017-z
Ibuprofen	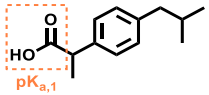	IBU	$C_{13}H_{18}O_2$	206.28	4.4 ($pK_{a,1}$)	*Chem. Eng. J.* 277 (2015) 360, doi: 10.1016/j.cej.2015.04.097
Naproxen	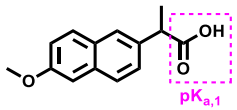	NPX	$C_{14}H_{14}O_3$	230.26	4.2 ($pK_{a,1}$)	*J. Pharm. Biomed. Anal.* 42 (2006) 126, doi: 10.1016/j.jpba.2005.11.029

Table S7. Adsorption capacity of other adsorbents reported in previous literature data, to the adsorptive removal of tetracycline and other selected pharmaceuticals studied in this work.

Adsorbent	Type of adsorbent	Adsorbent loading [g/L]	C_o [mg/L]	pH	Temp. [°C]	Time [min]	Adsorption capacity (q_e) [mg/g]	References
Tetracycline								
CPS	Agriculture waste coated with zinc oxide	200.0-10000.0	30-70	3.0-9.0	25-35	0-120	99	*Arab. J. Chem.* 13 (2020) 4629, doi:10.1016/j.arabjc.2019.10.010
Zn-BTC@SBC	Metal-organic framework porous biochar composite	0.4	20	3.0-11.0	25	1440	126	*J. Mol. Liq.* 384 (2023) 122283, doi:10.1016/j.molliq.2023.122283
HCP-N/S-2	Hyper-cross-linked polymer	5.0	50	6.0	25	180	138	*Mater. Sci. Eng. B* 303 (2024) 117335, doi: 10.1016/j.mseb.2024.117335
PMGO	Magnetic graphene oxide nanocomposite	0.2	22-71	2.0-10.0	25	-	194	*React. Funct. Polym.* 191 (2023) 105701, doi:10.1016/j.reactfunct-polym.2023.105701
NaY zeolite	Zeolite	500.0	80	7.0	30	1440	202	*J. Clean. Prod.* 172 (2018) 602, doi:10.1016/j.jclepro.2017.10.180
SKTPS	Hyper-cross-linked polymer	1.0	0.044	7.0	RT	5	209	*ACS Appl. Mater. Interfaces.* 14 (2022) 7369, doi:10.1021/acsami.1c24393
HCP-BPA-Na	Hyper-cross-linked polymer	0.075	0.125	3.0	25-45	-	268	*J. Water Process Eng.* 40 (2021) 101902, doi:10.1016/j.jwpe.2020.101902
HCP-MAH	Hyper-cross-linked polymer	0.125	30	7.0	25	1440	273	*J. Environ. Chem. Eng.* 9 (2021) 106047, doi:10.1016/j.jece.2021.106047
La-impregnated MCM-41	Zeolite	0.06	100	7.0	RT	1440	303	*Environ. Technol.* 31 (2010) 233, doi:10.1080/09593330903453210

ZIF-8	Metal-organic framework	0.5	50	4.0	30	240	313	*J. Hazard. Mater.* 366 (2019) 563, doi:10.1016/j.jhazmat.2018.12.047
CRAC@Fe_2O_3	Magnetic activated carbon	0.05-0.5	50	2.0-10.0	30	300	313	*Chemosphere* 310 (2023) 136892, 10.1016/j.chemosphere.2022.136892
P1-HCP	**Hyper-cross-linked polymer**	**0.05**	**20**	**4.5**	**RT**	**1440**	**330**	**This work**
sHCP1	Hyper-cross-linked polymer	0.025	15	6.5	RT	180	413	*J. Environ. Chem. Eng.* 11 (2023) 110429, doi:10.1016/j.jece.2023.110429
HCP-COOH	Hyper-cross-linked polymer	0.125	30	7.0	25	1440	418	*J. Environ. Chem. Eng.* 9 (2021) 106047, doi:10.1016/j.jece.2021.106047
Cu-MOF@ Co-MOF	Bimetallic organic framework	0.5	10-450	2.0-11.0	25-45	0.5-25	435	*Sci. Rep.* 14 (2024) 17607, doi:10.1038/s41598-024-67986-8
MB_{CP}	Modified bentonite	0.2	100	6.0	25	0-90	476	*Sep. Purif. Technol.* 274 (2021) 119059, doi:10.1016/j.seppur.2021.119059
				Ciprofloxacin				
MgO/Chit/GO	Chitosan-based nanocomposite	0.5	30-1500	7.0	25	360	23	*Microchim. Acta.* 186 (2019) 459, doi:10.1007/s00604-019-3563-x
Chit/CNT	Chitosan-carbon nanotubes hydrogel beads	1.5	40	7.0	RT	720	24	*J. Hazard. Mater. Adv.* 13 (2024) 100404, doi: 10.1016/j.hazadv.2024.100404
PIM-1	Polymer of intrinsic microporosity	0.4	73	7.0	RT	1440	31	*Sci. Rep.* 10 (2020) 1, doi:10.1038/s41598-020-57616-4
poly(styrenesulfonate)/Al_2O_3	Polyelectrolyte	5.0	10	6.0	RT	90	35	*J. Mol. Liq.* 309 (2020) 113150, doi:10.1016/j.molliq.2020.113150
CBHB	Chitosan-based hydrogel	0.25	50	3.0	30	-	37	*Sci. Total Environ.* 639 (2018) 560, doi:10.1016/j.scitotenv.2018.05.129

CS/MMT/ZnO	Nanocomposite	0.03	30	7.0	RT	120	57	*J. Water Process Eng.* 63 (2024) 105449, doi: 10.1016/j.jwpe.2024.105449
JLUE-HCOPs	Covalent organic framework	1.0	20	6.0	RT	2880	84	*Eur. Polym. J.* 123 (2020) 109445, doi:10.1016/j.eurpolymj.2019.109445
CPS	Agriculture waste coated with zinc oxide	0.2-10	30-70	3.0-9.0	25-35	120	92	*Arab. J. Chem.* 13 (2020) 4629, doi:10.1016/j.arabjc.2019.10.010
CaMgAl-LDH/RM	Nanocomposite	5	70	7.0	RT	90	138	*Results Eng.* 23 (2024) 102600, doi: 10.1016/j.rineng.2024.102600
GH	Porous graphene hydrogel	-	50	6.0	25	-	236	*Sci. Rep.* 5 (2015) 1, doi: 10.1038/srep13578
Fe_3O_4/graphene/ bentonite clay	Nanocomposite	0.01	10	5.0	-	110	237	*Inorg. Chem. Commun.* 174 (2025) 113991, doi: 10.1016/j.inoche.2025.113991
P1-HCP	**Hyper-cross-linked polymer**	**0.05**	**20**	**4.5**	**RT**	**1440**	**300**	**This work**
GO	Graphene oxide	0.125	50	5.0	25	180	354	*Chem. Eng. J.* 487 (2024) 150484, doi: 10.1016/j.cej.2024.150484
sHCP1	Hyper-cross-linked polymer	0.025	15	6.5	RT	180	428	*J. Environ. Chem. Eng.* 11 (2023) 110429, doi:10.1016/j.jece.2023.110429
MB_{CP}	Modified bentonite	0.2	100	6.0	25	90	457	*Sep. Purif. Technol.* 274 (2021) 119059, doi:10.1016/j.seppur.2021.119059
spherical MgO	Metal-based nanomaterial	0.1	25	9.0	RT	50	~460	*J. Environ. Chem. Eng.*8 (2020) 104256, doi: 10.1016/j.jece.2020.104256
sHCP(1:4)	Hyper-cross-linked polymer	0.025	30	6.8	RT	180	758	*Sep. Purif. Technol.* 343 (2024) 127147, doi: 10.1016/j.seppur.2024.127147
nickel sulphide/ L-glutathione	Nanomaterial	0.333	50	4.5	RT	1440	972	*Colloids Surf. A Physicochem. Eng. Asp.* 586 (2020) 124264, doi: 10.1016/j.colsurfa.2019.124264
				Diclofenac				
ZN	Natural zeolite	2.000	20	2.0	20	120	~8	*CSCEE* 9 (2024) 100575, doi: 10.1016/j.cscee.2023.100575

fibrous silica KCC-1	Silica-based composite	1.000	160	4.0	RT	40	65	*J. Environ. Chem. Eng.* 11 (2023) 111295, doi: 10.1016/j.jece.2023.111295
MWCNT-OH/COOH-Fe@coffee	Functionalized carbon nanotubes	1.500	119	~7.0	RT	20	77	Environ. Res. 251 (2024) 118733, doi: 10.1016/j.envres.2024.118733
HCP-N/S-2	Hyper-cross-linked polymer	5.000	50	6.0	25	180	141	*Mater. Sci. Eng. B* 303 (2024) 117335, doi: 10.1016/j.mseb.2024.117335
P1-HCP	**Hyper-cross-linked polymer**	**0.05**	**20**	**4.5**	**RT**	**1440**	**159**	**This work**
sycamore ball activated carbon	Activated carbon	0.200	10-50	~4.0	25	210	179	*Surf. Interfaces* 24 (2021) 101097, doi: 10.1016/j.surfin.2021.101097
P-POP-2	Porous organic polymer	0.1	15	5.0	RT	180	217	*Chem. Eng. J.* 379 (2020) 122290, doi: 10.1016/j.cej.2019.122290
cogon grass-derived CNF/GnP aerogel	Nanocomposite	4.5	10	4.0	RT	-	219	*J. Mol. Liq.* 419 (2025) 126760 doi: 10.1016/j.molliq.2024.126760
ALB85	Amine functionalized egg albumin hydrogel	0.500	10-300	~6.0	N/A	180	233	*J. Haz. Mat.* 393 (2020) 122417, doi: 10.1016/j.jhazmat.2020.122417
COF-3-NH_2	Covalent Organic Framework	0.040	25	5.0	25	180	300	*Chem. Eng. J.* 459 (2023) 141561, doi: 10.1016/j.cej.2023.141561
UiO-66-$(COOH)_2$	Zirconium-based Metal-organic Framework	2.000	100-4000	7.0	25	4 320	481	*J. Colloid Interface Sci.* 607 (2022) 334, doi: 10.1016/j.jcis.2021.08.158
HCP1-N	Hyper-cross-linked polymer	0.025	15	4.0	RT	360	544	*Environ. Res.* 268 (2025) 120791, doi: 10.1016/j.envres.2025.120791
MOF-808	Metal Organic Framework	0.500	0.6	5.5	RT	1440	800	*Chem. Eng. J.* 417 (2021) 129216, doi: 10.1016/j.cej.2021.129216
				Ibuprofen				

AT-MC	Biosorbent	6	500	6.0	~45	~45	37	*Case Stud. Chem. Environ. Eng.* 9 (2024) 100718, doi: 10.1016/j.cscee.2024.100718
LF@ppy@LDH	Nanocomposite	-	200	5.0	25	-	44	*Heliyon* 11 (2025) e40783, doi: 10.1016/j.heliyon.2024.e40783
$NiFe_2O_4$@SiO_2 @APTS	Nanocomposite	0.1	6-14	7.0	RT	30	59	*J. Clean. Prod.* 294 (2021) 126155, doi: 10.1016/j.jclepro.2021.126155
HCP1-N	Hyper-cross-linked polymer	0.025	15	6.0	RT	360	128	*Environ. Res.* 268 (2025) 120791, doi: 10.1016/j.envres.2025.120791
P1-HCP	**Hyper-cross-linked polymer**	**0.05**	**20**	**4.5**	**RT**	**1440**	**140**	**This work**
AC HP with HTCa	Activated carbon	0.4	200	6.5	25	480	204	*J. Ind. Eng. Chem.*, doi: 10.1016/j.jiec.2025.02.060
TFPB-Dg_{Cl}-COF	Covalent organic framework	0.125	100	5.0	RT	180	~300	*Colloids Surf. A: Physicochem. Eng. Asp* 685 (2024) 133309, doi: 10.1016/j.colsurfa.2024.133309
Cu-doped Mil-101(Fe)	Metal-organic Framework	0.1	20	3.0-11.0	RT	180	497	*Sci. Total Env.* 797 (2021) 149179, doi: 10.1016/j.scitotenv.2021.149179
IB-COF	Covalent Organic Framework	0.5	50	4.0	RT	60	512	*J. Hazard. Mat. Adv.* 15 (2024) 100451, doi: 10.1016/j.hazadv.2024.100451
				Naproxen				
Gel-1.0MOF-Sep	Biosorbent composite aerogel	-	10	7.0	20	720	~2	*Chem. Eng. J.* 452 (2023) 139426, doi: 10.1016/j.cej.2022.139426
Al-MOF-Fe_3O_4@P4VP	Metal-organic framework	1	20	4.7	20	120	32	*J. Hazard. Mater.* 383 (2020) 121144, doi: 10.1016/j.jhazmat.2019.121144
β-CD/rGO	Cyclodextrin and graphene oxide-based composite	0.1	10	6.5	40	360	~45	*Chem. Eng. J* 412 (2021) 128710, doi: 10.1016/j.cej.2021.128710
HKUST-1/ZnO/SA	Metal-organic framework	0.2	80	6.0	25	120	80	*Sustain. Chem. Pharm.* 29 (2022) 100757, doi: 10.1016/j.scp.2022.100757
UiO-66	Metal-organic frameworks	0.05	9	4.4	25	600	89	*Chem. Eng. J.* 360 (2019) 645, doi: 10.1016/j.cej.2018.12.021

HCP1-N	Hyper-cross-linked polymer	0.025	15	6.0	RT	360	102	*Environ. Res.* 268 (2025) 120791, doi: 10.1016/j.envres.2025.120791
P1-HCP	**Hyper-cross-linked polymer**	**0.05**	**20**	**4.5**	**RT**	**1440**	**117**	**This work**
GTFPAC	Activated carbon	0.5	100	4.0	25	180	129	*J. Environ. Chem. Eng.* 9 (2021) 106820, doi: 10.1016/j.jece.2021.106820
Cu-doped Mil-101(Fe)	Metal-organic framework	0.1	20	-	RT	180	178	*Sci. Total Environ.* 797 (2021) 149179, doi: 10.1016/j.scitotenv.2021.149179

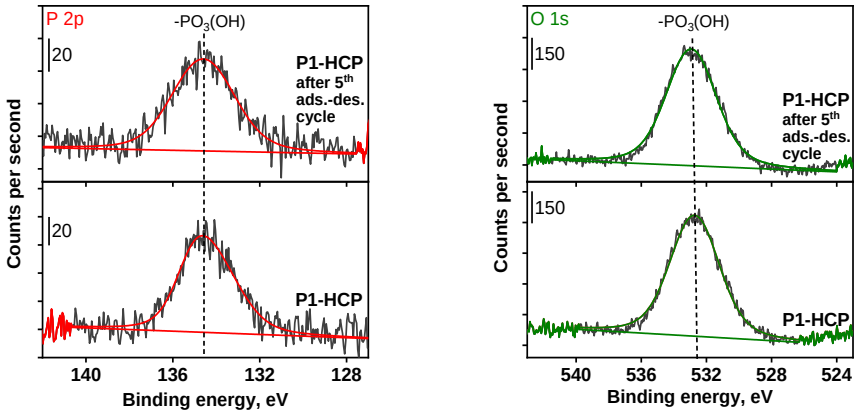

Fig. S12. Comparison of XPS spectra of fresh P1-HCP and P1-HCP after 5th adsorption-desorption (ads.-des.) cycle in the P 2p and O 1s binding energy ranges.